https://doi.org/10.5194/egusphere-2025-2785
Preprint. Discussion started: 16 July 2025

Diurnal Asymmetry in Nonlinear Responses of Canopy Urban Heat Island to Urban Morphology in Beijing during Heat Wave Periods

Tao Shi[1,2,3,4], Yuanjian Yang[5*], Ping Qi[1], Simone Lolli[6]

[1]School of Mathematics and Computer Science, Tongling University, Tongling, 244000, China
[2]Anhui Province Key Laboratory of Physical Geographic Environment, Chuzhou University, Chuzhou, 239000, China
[3]Anhui Engineering Research Center of Remote Sensing and Geoinformatics, Chuzhou, 239000, China
[4]Anhui Center for Collaborative Innovation in Geographical Information Integration and Application, Chuzhou, 239000, China
[5]State Key Laboratory of Climate System Prediction and Risk Management, School of Atmospheric Physics, Nanjing University of Information Science and Technology, Nanjing 210044, China
[6]CNR-IMAA, Contrada S. Loja, 85050 Tito Scalo (PZ), Italy

Correspondence to: Prof. Yuanjian Yang (yyj1985@nuist.edu.cn)

Abstract. Currently, the diurnal asymmetric mechanism by which urban morphology affect canopy urban heat island (CUHI) during heat wave (HW) periods has not received sufficient attention. This study took the area within the Fifth Ring Road in Beijing as the research object, integrating XGBoost machine learning model and ENVI-met microclimate simulation technology to quantitatively analyze the non-linear response characteristics of CUHII to urban morphology during HW periods. The results show that CUHI intensity (CUHII) during HW periods is significantly enhanced compared with non-heat wave (NHW) periods, with a daytime increase of 91.3% and a nighttime increase of 52.7%. The analysis of the XGBoost model indicates that the building coverage ratio (BCR) is the core driving factor of CUHII during the day, while the sky view factor (SVF) plays a more prominent dominant role at night. The regulatory effects of 2D/3D morphological indicators during HW periods are significantly stronger than during NHW periods. ENVI-met simulations further reveal the nonlinear regulation mechanism of building height on diurnal thermal environments: as SVF decreases, daytime thermal environments are collaboratively driven by short-wave radiation shading and ventilation resistance, while nighttime thermal environments are dominated by the reflection and accumulation of long-wave radiation by buildings. Furthermore, this study explores the regulatory effect of the wind environment on CUHII and its diurnal differences. The findings of this study provide new insights into the formation mechanisms of diurnal differences in CUHII and offer a scientific basis for the optimal design of urban morphological indicators under extreme high-temperature conditions.

1 Introduction

The latest assessment report from the Intergovernmental Panel on Climate Change (IPCC) indicates a significant increase in the frequency, intensity, and duration of extreme heat events (IPCC, 2021). The CUHI, the phenomenon of abnormal air temperature from near-surface to roof height, has become a research focus due to its direct impact on outdoor thermal comfort and building energy consumption (Battista et al., 2023; Shi et al., 2024). Notably, in particular, the CUHII is

https://doi.org/10.5194/egusphere-2025-2785
Preprint. Discussion started: 16 July 2025

amplified significantly during HW periods. In megacities such as Beijing, Shanghai and Guangzhou, China, the intensity of canopy heat island increases by 0.8 to 1.2 ° C during HW periods (Jiang et al., 2019; Yang et al., 2023), with a marked expansion in diurnal amplitude (Ao et al., 2019; Shi et al., 2024).

Against the backdrop of urban heat island mitigation, deciphering the mechanism by which complex urban morphology drives local thermal environments is of critical scientific significance (Berger et al., 2017; Huang & Wang, 2019; Wu et al., 2022; Guo et al., 2023). Existing studies show that two-dimensional urban morphological indicators (e.g., building area ratio, aggregation index) are key controlling factors for local thermal environments (Henits et al., 2017; Shi et al., 2021). With the widespread use of three-dimensional building data (e.g., building height, SVF), research confirms that three-dimensional morphological indicators such as building height, SVF exhibit stronger explanatory power for local thermal environments (Shao et al., 2023; Zhang et al., 2023; Ding et al., 2024). Although there are conflicting conclusions regarding the correlation between three-dimensional morphological elements and thermal environments (e.g., SVF showing a positive, negative, or no significant correlation with local temperature) (Huang & Wang, 2019; Li & Hu, 2022), their inclusion in models can enhance the explanatory power of urban heat island intensity by up to 20% (Wu et al., 2022). However, existing studies have not clarified the impacts of 2D/3D morphology on daytime and nighttime CUHII and their driving mechanisms, and systematic analysis during HW periods is even more lacking.

Current research on the nonlinear relationship between urban morphology and local thermal environments focuses primarily on surface thermal environments (Han et al., 2022; Wu et al., 2022; Guo et al., 2023; Gu et al., 2024; Wang et al., 2024; Liu et al., 2025). For example, Gu et al. (2024) found that the enhancement effect of floor area ratio on land surface temperature tends to saturate when floor area ratio exceeds 0.6, and the impact of building height on LST slows when building height exceeds 15 meters. In particular, due to fundamental differences in physical mechanisms between the air temperature of the urban canopy (based on the thermodynamic processes of the canopy air) and the surface temperature (based on the energy balance of surface radiation), these conclusions cannot be applied directly to CUHI research. Traditional statistical models such as Ordinary Least Squares (Wang et al., 2020), Spatial Autocorrelation Model (Fallah Ghalhari and Dadashi Roudbari, 2018), and Geographically Weighted Regression (Gao et al., 2022) have inherent limitations in handling nonlinear relationships (Alonso & Renard, 2020), while machine learning methods – through feature importance analysis and SHAP value interpretation (Lundberg & Lee, 2017) – offer a new technical approach. Furthermore, ENVI-met, a three-dimensional non-hydrostatic model, enables microclimate simulation at 0.5–10 m spatial resolution and 1–10 s temporal resolution by coupling short/long-wave radiation budget processes on building surfaces (Chan & Chau, 2021), providing a powerful tool for fine-scale analysis of regional microclimate mechanisms (Meng et al., 2024; Luo et al., 2024).

Beijing, as a typical fast-developing megacity, exhibits significant spatial heterogeneity in urban morphology due to its polycentric ring development pattern (Jiang et al., 2024), offering an ideal case for studying diurnal differences in CUHII during HW periods. This study integrates ground observation data and high-precision urban morphology data, combining machine learning and numerical simulation methods to systematically explore the contributions of key three-dimensional urban morphological indicators to CUHII during HW periods and the diurnal variations in their nonlinear modulation. The

https://doi.org/10.5194/egusphere-2025-2785
Preprint. Discussion started: 16 July 2025

findings will not only provide quantifiable morphological indicators for the management of urban extreme heat risk, but will also provide scientific information on the diurnal variations of CUHII and their potential causes.

2 Data and methodology

2.1 Study Area

Beijing megacity is located at the northern end of the North China Plain, featuring a complex terrain: the Yan Mountain and Taihang Mountain with altitudes exceeding 2000 meters adjoin theirnorth and west, the northeast is hilly, the south is plain, and the southeast extends to the Bohai Bay to form a land-sea transition zone. From 1978 to 2022, Beijing's population increased from 8.71 million to 21.84 million, with 41.8% of the permanent population concentrated within the Fifth Ring Road, which accounts for only 4.07% of the city's area, demonstrating significant population agglomeration. This study focuses on the area within the fifth ring road (Figure 1). As central urbanization area of Beijing, the spatial heterogeneity of population density, building distribution, and green space configuration in this region provides a typical scenario for urban thermal environment research. Although the urban green coverage rate increased from 22.3% in 1978 to 49.0% in 2020, the intensity of the heat island still increased at a rate of 0.24℃/year (Ge et al., 2016). Based on the land surface temperature data during the NHW and HW periods in summer, this study focuses on analyzing the diurnal variations of CUHII and exploring its correlation mechanism with urban morphology.

https://doi.org/10.5194/egusphere-2025-2785
Preprint. Discussion started: 16 July 2025

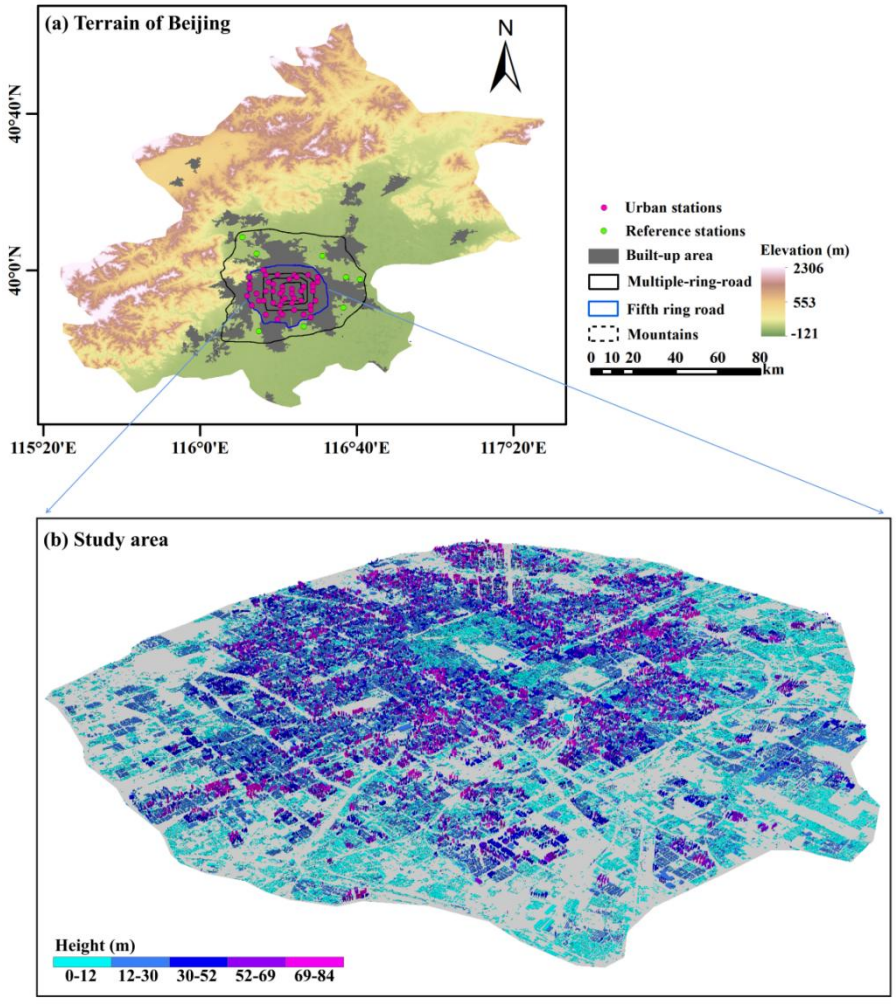

Figure 1: Overview of the study area. Overview of the study area. (a) Topography and land use in Beijing, with distribution of urban and reference observation stations in the built-up area of the city. (b) Urban morphological characteristics of the study region.

2.2 Data collection and processing

2.2.1 AWS observation data

The hourly observation data from automatic weather stations (AWS) used in this study were obtained from the China Meteorological Data Service Center (http://data.cma.cn/en), including meteorological elements such as near-surface air temperature, wind speed, wind direction, humidity, and precipitation. To ensure data accuracy, we performed quality control on the ground station observation data: referring to previous research methods (Yang et al., 2011; Xu et al., 2013), we imputed missing values in the observation sequences using the average of synchronous observation data from the five

https://doi.org/10.5194/egusphere-2025-2785
Preprint. Discussion started: 16 July 2025

nearest stations around the site and excluded station records with excessive errors. The final AWS observation dataset from 2018-2022 was used to analyze the spatio-temporal distribution characteristics of the near-surface thermal field in the Beijing megacity.

2.2.2 Selection and calculation of urban morphology indicators

Existing studies have used multidimensional indicators to characterize the spatial structure of cities. Two-dimensional (2D) morphological indicators include BCR (Yin et al., 2018) and floor area ratio (FAR), etc. Three-dimensional (3D) morphological indicators cover average building height (H, Tian et al., 2019), sky view factor (SVF, Scarano & Mancini, 2017), etc. We obtained building data from Baidu Maps (https://map.baidu.com), including building base projection boundaries and total floor information. We calculate the height of the building by multiplying the number of floors by 3 meters. This method has been verified to have an overall accuracy of 86.78% (Liu et al., 2021), and the conversion results are reliable based on the regular characteristics of the floor heights of urban buildings (Alavipanah et al., 2018). In this study, we selected six 2D indicators and six 3D indicators to measure the morphological characteristics of the building within a 500 meter buffer around the AWS (Oke, 2004). The definitions and calculations of the specific indicators are as follows in Table S1.

2.3 Method implementation

2.3.1 NHW and HW periods classification

Global standards for defining HW events vary significantly due to climatic backgrounds, geographical conditions, and socioeconomic factors. The World Meteorological Organization (WMO) defines a heat wave as three consecutive days with maximum temperatures exceeding 32°C; the National Oceanic and Atmospheric Administration (NOAA) uses a heat wave index that integrates temperature and humidity, issuing alerts when the index exceeds 40.5°C for at least three hours per day for two consecutive days or forecasts reach 46.5°C; the Royal Netherlands Meteorological Institute requires five consecutive days with maximum temperatures over 25°C, including at least three days exceeding 30°C. This study adopts the China Meteorological Administration (CMA) definition of heat waves as three consecutive days with maximum temperatures ≥35°C. Considering that maximum temperatures at urban stations may be influenced by urbanization, we identify heat waves based on reference station data in this study: In summer, a day is classified as a HW day if more than two reference stations simultaneously meet the CMA heat wave criteria; otherwise, it is a NHW day (Yang et al., 2023; Xue et al., 2023).

2.3.2 CUHII quantification

Academia typically defines CUHII as the temperature difference between urban and reference stations (Yang et al., 2023; Shi et al., 2024). The selectionof reference stations is critical for the calculation of CUHII, adhering to specific criteria: 1) Significantly lower temperatures than urban stations; 2) Location in rural forest-shrub areas more than 50 km from the city center (Yang et al., 2023); 3) Uniform distribution in different urban orientations. Finally, we selected 8 reference stations (green markers in Figure 1), with an average altitude of 39.6 m, 8.8 m lower than the 45 urban stations (red markers in

https://doi.org/10.5194/egusphere-2025-2785
Preprint. Discussion started: 16 July 2025

Figure 1). We obtained summer CUHII values for urban stations by calculating temperature differences between urban and reference stations.

2.3.3 Machine learning model

Compared to traditional machine learning methods, the XGBoost algorithm demonstrates significant advantages in accuracy, flexibility, anti-overfit capability, and missing value processing (Chen et al., 2023). Its superior performance stems from loss function optimization based on second-order Taylor expansion, multithread parallel computing support, and regularization constraint mechanisms (Chen & Guestrin, 2016). Existing studies show that nonlinear relationships universally exist between various influencing factors and thermal environments (Lin et al., 2024). Traditional linear regression models struggle to capture the nonlinear local characteristics between influencing factors and thermal environments, while XGBoost can effectively analyze the nonlinear mechanism between factor changes and local thermal environments (He et al., 2024). Additionally, we introduce the SHAP model in this study to improve interpretability, which quantifies the impact of each morphological parameter on the thermal environment through global and local variable attribution (Hong et al., 2025). By combining partial dependency plots (PDP) to visualize the functional relationship between feature variables and model outputs, we clarify the marginal effects of urban morphological indicators on CUHII, supporting the identification of key driving factors and their threshold characteristics.

2.3.4 ENVI-met Model setup and initialization

ENVI-met has been widely applied in the assessment of cooling effect (Di Giuseppe et al., 2021), temperature field prediction (Forouzandeh, 2021), and thermal comfort research (Berardi et al., 2020). The model integrates high-resolution Google Earth imagery and field survey data to accurately construct the three-dimensional spatial configuration of buildings, vegetation, and soil, with vegetation parameters derived from ENVI-met's 3D plant database. The horizontal extent of the model is set to 1×1 km (200×200 grids, 5 m resolution), and the vertical direction has 65 layers of grids. To reduce boundary effects, we used a 10-layer nested grid technique (Kong et al., 2016), setting surface materials as a mixture of loam and asphalt. We update model boundary meteorological parameters (temperature, humidity, wind speed, wind direction) every 30 minutes using a complete forcing method, with data from meteorological station measurements. For model validation, we use two indicators: coefficient of determination (R^2) and root mean square error (RMSE), focusing on the simulation accuracy of the air temperature at 1.5 m height. We select typical urban meteorological stations in Beijing, design multi-scenario simulation schemes, and emphasize analyzing the mechanism of morphological indicators on CUHII, canopy ventilation, and radiation exchange.

3 Results

3.1 Diurnal variations of CUHII during HW periods

Under climate warming, urban expansion has increased built areas, with human activities generating additional anthropogenic heat and pollutant emissions that intensify urban warming. Using observational data from Beijing's AWS, this study examines the diurnal variations of CUHII during both heatwave and non-heatwave periods.

https://doi.org/10.5194/egusphere-2025-2785
Preprint. Discussion started: 16 July 2025

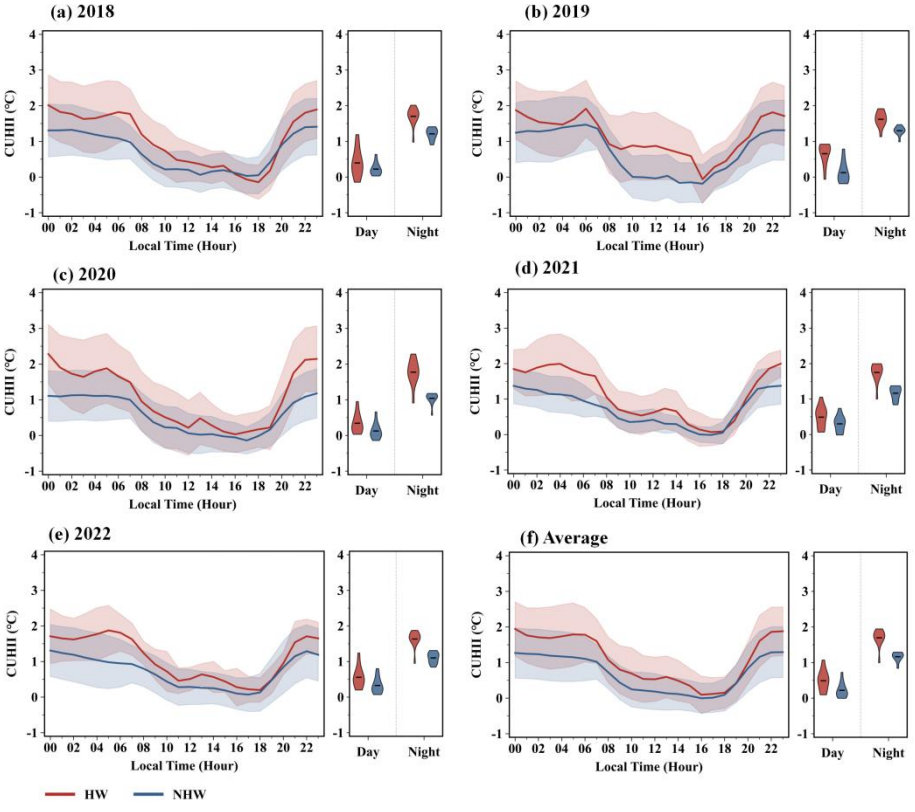

Figure 2: Diurnal variations of the CUHII during the NHW and HW periods. (a)-(e) Year-specific patterns; (f) Multi-year average. Left panels: CUHII diurnal cycles (solid lines) with shaded areas showing standard deviations. Right panels: Violin plots of CUHII distributions during the day (08:00-19:00) and at night (00:00-07:00, 20:00-24:00).

In Figure 2, the summer diurnal variations of CUHII in Beijing megacity during HW periods exhibit a U-shaped fluctuation. CUHII begins to decline gradually at 06:00 Beijing Time (BJT), reaches the lowest value at 16:00 BJT, then gradually rebounds, and remains at a high level from 22:00 BTJ to 05:00 BJT the next day. The diurnal variation trend of CUHII during NHW periods is generally consistent with that during HW periods. In particular, except for 19:00 BJT 2018 (Figure 2c), the hourly CUHII values during HW periods in each year are higher than those during NHW periods. From the annual average (Figure 2f), CUHII during the HW periods ranges from 0.18 to 2.06 ° C, significantly higher than 0.03 to 1.32 ° C during the NHW periods, indicating a significant intensification of CUHII during the HW periods compared to the NHW periods (Cheval et al., 2024; Shi et al., 2024).). The violin plots clearly show the diurnal distribution characteristics of CUHII during the HW (red) and NHW (blue) periods: during the day, the mean CUHII during the HW periods is 0.54 ° C, slightly higher than 0.23 ° C during the NHW periods; at night, the median CUHII during the HW periods reaches 1.71 ° C, with a more significant increase than 1.12 ° C during the NHW periods. It should be noted that the violin plot during the nighttime HW period shows a narrower and shorter distribution, indicating that CUHII values are more concentrated and the

https://doi.org/10.5194/egusphere-2025-2785
Preprint. Discussion started: 16 July 2025

overall range is smaller. This phenomenon may be related to the enhanced stability of the urban thermal environment at night (Gosling et al., 2009; Shi et al., 2021).

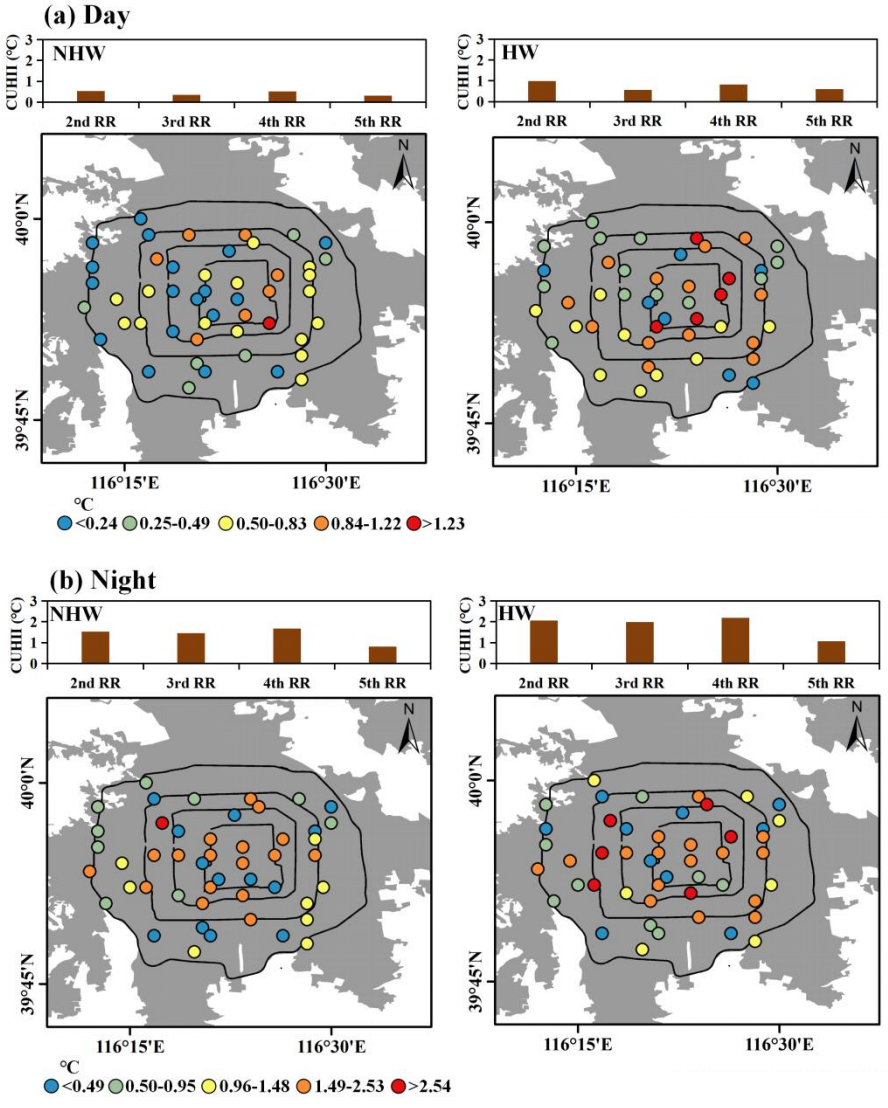

180 **Figure: 3 Diurnal spatial patterns of CUHII during NHW and HW periods. (a)-(e) Year-specific patterns; (f) Multi-year average. Different colored dots represent different ranks of the CUHII.**

Beijing megacity has experienced rapid and large-scale urbanization over the past few decades, with urban spaces continually expanding to the suburbs, leading to a significant CUHI effect (Zheng et al., 2018). The spatial analysis of
185 daytime CUHII shows (Figure 3a) thatthe econd ring having the highest CUHII (0.52℃ during NHW periods and 0.99℃ during HW periods), followed by the Fourth Ring (0.51℃ during NHW periods and 0.82℃ during HW periods). The

https://doi.org/10.5194/egusphere-2025-2785
Preprint. Discussion started: 16 July 2025

nighttime CUHII differs (Figure 3b), with the Fourth Ring having the highest CUHII (1.68℃ during NHW periods and 2.19℃ during HW periods), followed by the Second Ring (1.53℃ during NHW periods and 2.06℃ during HW periods). The spatial pattern of the heat island effect formed during Beijing's urbanization process may be closely related to the morphological characteristics of the building. Analysis of urban configuration structures (Figure 4) shows that the Second Ring has the highest proportion of dense buildings (36.84%), while the Fourth Ring has the highest proportion of high-rise buildings (51.6%). The compact layout leads to the accumulation of solar radiation heat in dense building clusters during the day, which is difficult to diffuse (Ge et al., 2016), an important reason for improving CUHII at daytime. The concentrated release of artificial heat sources such as air conditioners in high-rise areas (Yin & Zhao, 2024) leads to the improvement of nighttime CUHII. These factors together result in the diurnal differences in the spatial pattern of CUHII in Beijing, and the causes will be further analyzed in combination with the morphological characteristics of the building below.

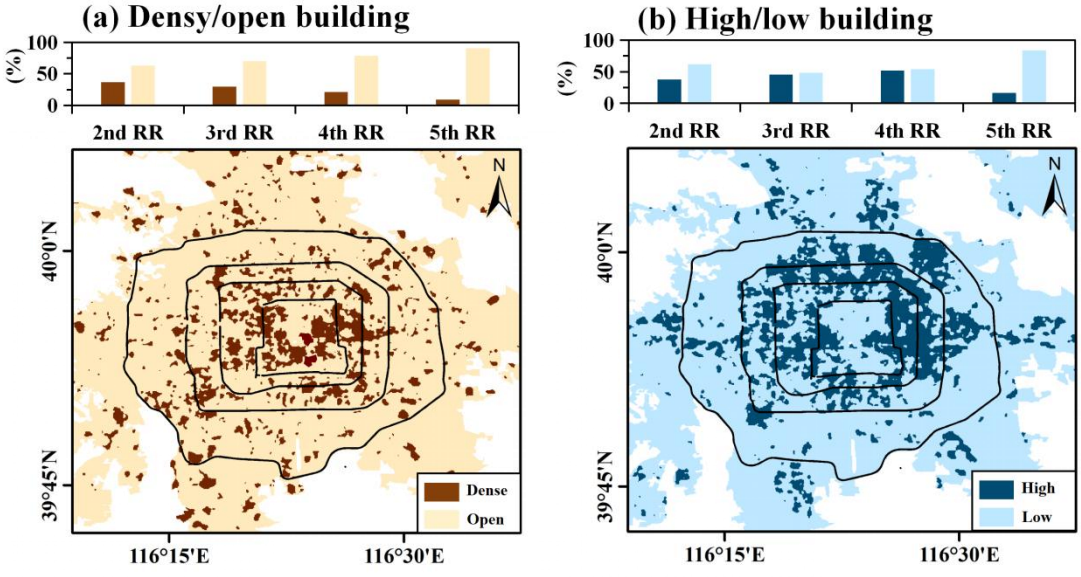

Figure: 4 (a) Urban configuration structures are dominated by density information, including dense and open rise. (b) Urban configuration structures are dominated by height information, including high-rise and low-rise.

3.2 Non-linear responses of CUHII to urban morphology

The spatial heterogeneity of urban morphology leads to an uneven distribution of near-surface air temperature by altering the surface energy balance and heat exchange processes. This section focuses on exploring the influence of urban morphological indicators on the diurnal spatial patterns of CUHII in Beijing megacity during HW periods.

https://doi.org/10.5194/egusphere-2025-2785
Preprint. Discussion started: 16 July 2025

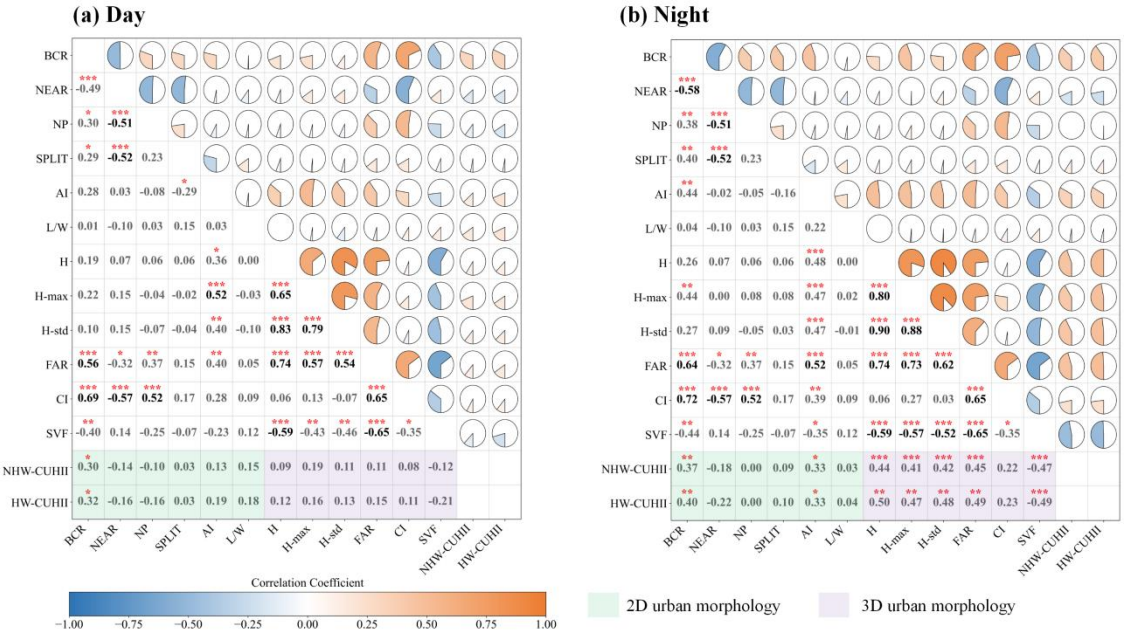

Figure: 5 Correlation coefficient matrix between urban morphology indicators and diurnal CUHII.

Figure 5a shows that, during the day, regardless of NHW or HW periods, the BCR among 2D morphological indicators exhibits the strongest correlation with CUHII. Among 3D indicators, the SVF shows the most significant negative correlation with CUHII. At night, the correlation between 2D indicators and CUHII significantly intensifies: for example, the correlation coefficient between BCR and CUHII increases from 0.37 during NHW periods to 0.40 during HW periods. In particular, the influence of 3D morphological indicators is markedly enhanced at night (Figure 5b): the negative correlation between SVF and CUHII is significantly strengthened (r = -0.47 during NHW periods, r=-0.49 during HW periods). The H, H_max, H_std, and FAR all show significant positive correlations with CUHII (r>0.41 during NHW periods, r>0.47 during HW periods). These results indicate that daytime CUHII is primarily regulated by the horizontal heterogeneity of urban morphology, while nighttime CUHII is driven mostly by vertical urban morphology. Furthermore, the correlations between morphological indicators and CUHII during the HW periods are generally higher than during the NHW periods.

https://doi.org/10.5194/egusphere-2025-2785
Preprint. Discussion started: 16 July 2025

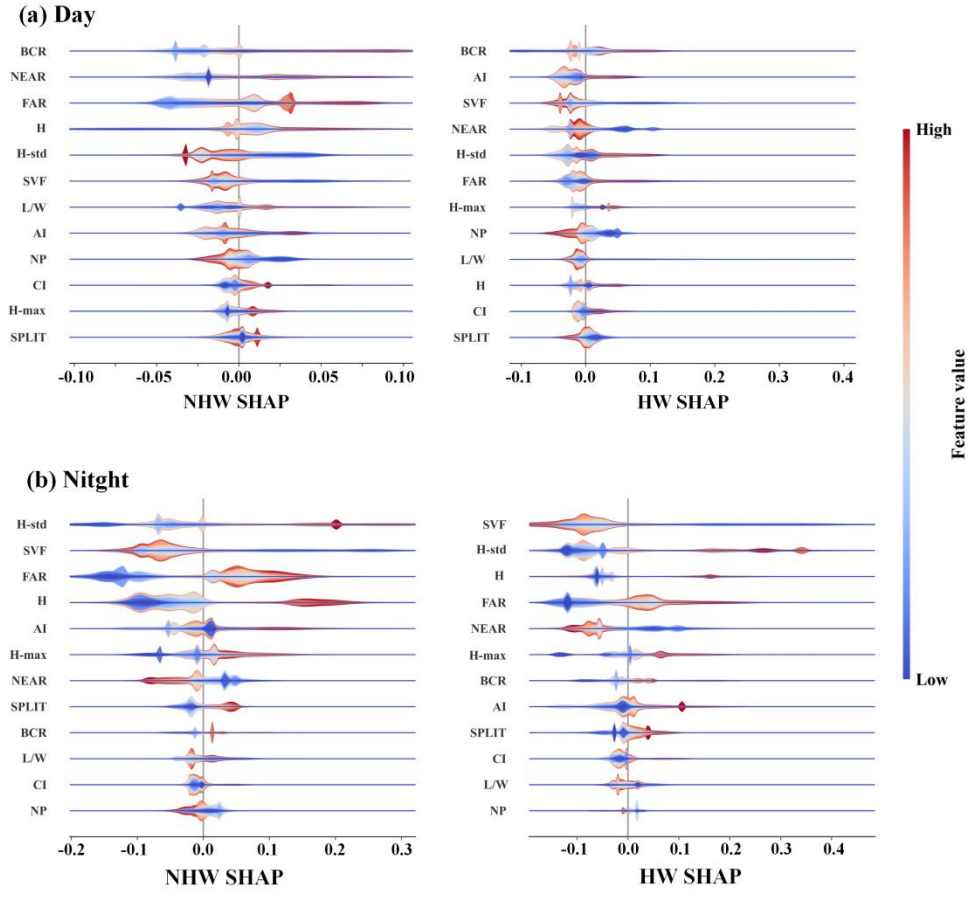

Figure 6: SHAP value analysis of urban morphology indicators for diurnal CUHII using XGBoost model.

The analyses based on Figures 6 and 7 indicate that: During daytime NHW periods, SHAP values of the 2D indicator BCR concentrate in the positive interval (left panel of Figure 6a), ranking first in importance (left panel of Figure 7a). This is because increased in building density leads to compact layouts and weakens the ventilation potential (Ng et al., 2011; Xu et al., 2019), with NEAR and FAR ranking second and third, respectively, and FAR showing a wider range of values. During daytime HW periods, the positive concentration trend of BCR becomes more significant (right panel of Figure 6a), maintaining its importance top- (right panel of Figure 7a). AI ranks second, while SVF shows an obvious negative deviation, consistent with the weak negative correlation observed in Figure 4 during the day. Furthermore, the mean SHAP values of the 2D indicators during the day are higher than those of the 3D indicators. Compared to NHW periods, the mean importance of 2D and 3D indicators during HW periods increases by 35.4% and 36.7%, respectively. At night during NHW periods, the dominance of 3D indicators begins to emerge: the SHAP value range of H_std expands significantly (left panel of Figure 6b), rising to the top in importance (left panel of Figure 7b), followed by SVF and FAR in the second and third positions, respectively. The BCR drops to the 9th position but remains positive. During nighttime HW periods, the dominance of 3D

https://doi.org/10.5194/egusphere-2025-2785
Preprint. Discussion started: 16 July 2025

indicators is further enhanced: the SHAP value range of SVF expands (right panel of Figure 6b), stably ranking first in importance (right panel of Figure 7b). High-rise residences, accompanied by high population density and air conditioning heat dissipation, exacerbate the heat island effect (Ryu & Baik, 2012). Compared to NHW periods, the mean importance of 2D and 3D indicators during HW periods increases by 16.2% and 31.3%, respectively. In summary, the dominant influencing factors of CUHII during the day are the urban 2D morphology, while the importance of the 3D morphology exceeds that of the 2D morphology at night. Heat wave events significantly enhance the importance of urban morphological indicators the impact of CUHII.

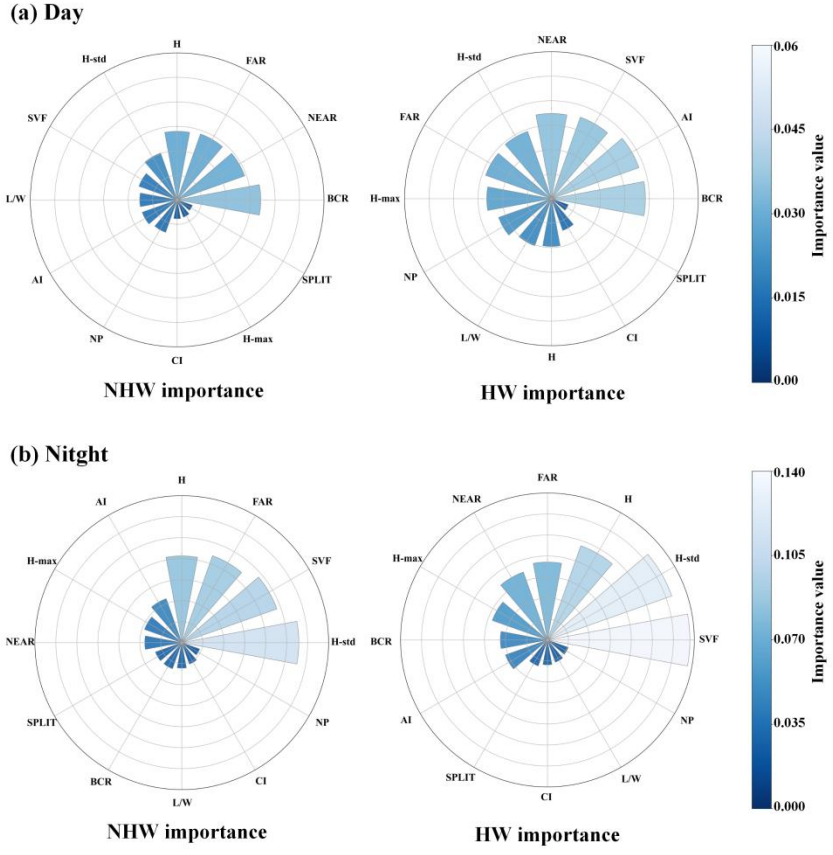

Figure 7: Importance value of urban morphology for diurnal CUHII during NHW and HW periods using XGBoost model.

Figure 8 reveals the dependency characteristics of urban morphology on CUHII: During the day, BCR shows nonlinear positive driving (left subplot of Figure 8a), with a significant threshold effect in the low-coverage interval (<0.12). The positive contribution growth rate slows when the BCR exceeds this value, and the threshold effect is more prominent during HW periods (Guo et al., 2016; Yang et al., 2018). SVF shows a negative effect in the interval of 0.725-0.735 and turns positive in the interval of 0.735-0.75 (middle subplot of Figure 8a), which may be related to the dual role of the height of the building in the thermal environment (Perini & Magliocco, 2014). Two-factor analysis shows (right subplot of Figure 8a) that

https://doi.org/10.5194/egusphere-2025-2785
Preprint. Discussion started: 16 July 2025

CUHII reaches its peak (yellow area) when BCR ≥ 0.23 and SVF ≤ 0.72, indicating that high BCR and low SVF synergistically exacerbate CUHII.At night, the increase in CUHII with the rise of BCR is more gentle than during the day (left subplot of Figure 8b), without obvious abrupt nodes, and the dominance of BCR weakens. SVF only shows negative regulation, and its intensity is higher than during the day (middle subplot of Figure 8b). Two-factor analysis indicates (right subplot of Figure 8b) that CUHII is the highest (yellow area) when BCR ≥ 0.23 and SVF ≤ 0.72, and the area of this region expands during HW periods. When SVF ≥ 0.75, the increase in BCR has a limited impact on CUHII, suggesting that high SVF can mitigate CUHII. In summary, the regulation of urban morphology in CUHII exhibits significant diurnal asymmetry: 2D indicators dominate during the daytime, while 3D indicators dominate at night. HW events can improve the non-linear modulation of urban morphological indicators.

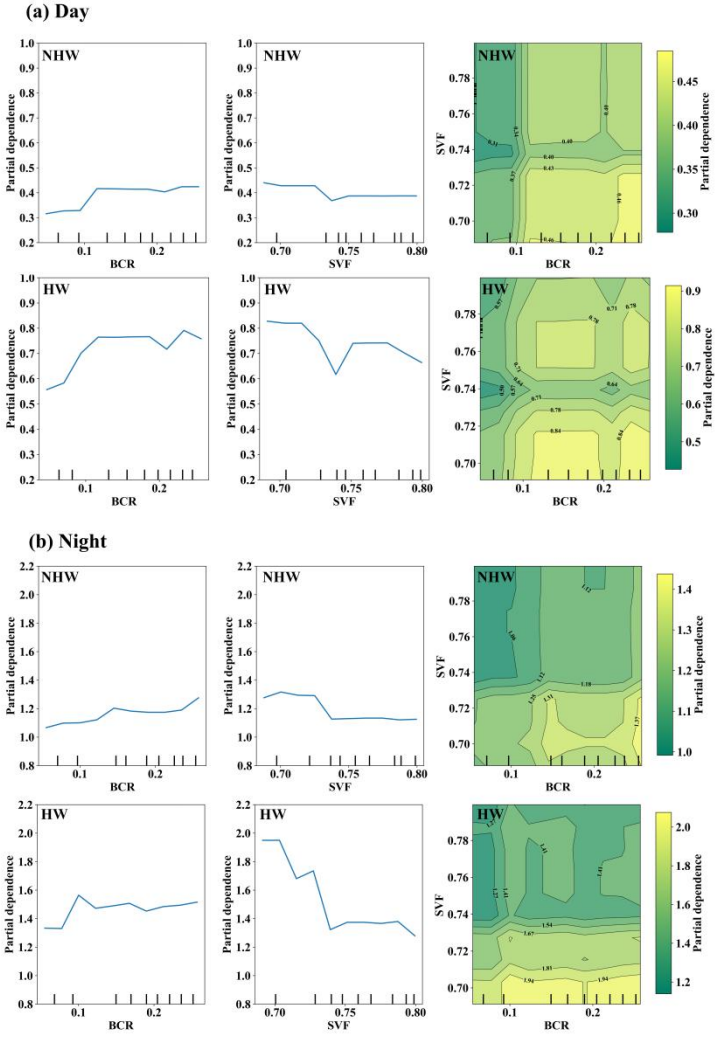

Figure: 8 Daytime and nighttime CUHII partial dependency plot (PDP) on urban morphology: the left subplot shows the PDP for BCR, the middle subplot shows the PDP for SVF, and the right subplot shows the two-way partial dependency plots for BCR and SVF.

https://doi.org/10.5194/egusphere-2025-2785
Preprint. Discussion started: 16 July 2025

3.3 Simulation of microclimate effects of key urban morphological indicators

This section draws on previous microclimate studies based on building morphology (Hu et al., 2022; Nugroho et al., 2022) and ensures scenario stability, using SVF as the 3D morphological indicator to conduct multi-scenario simulations via ENVI-met. The analysis focuses on exploring the influence mechanisms of SVF on the diurnal variations of local urban local environments.

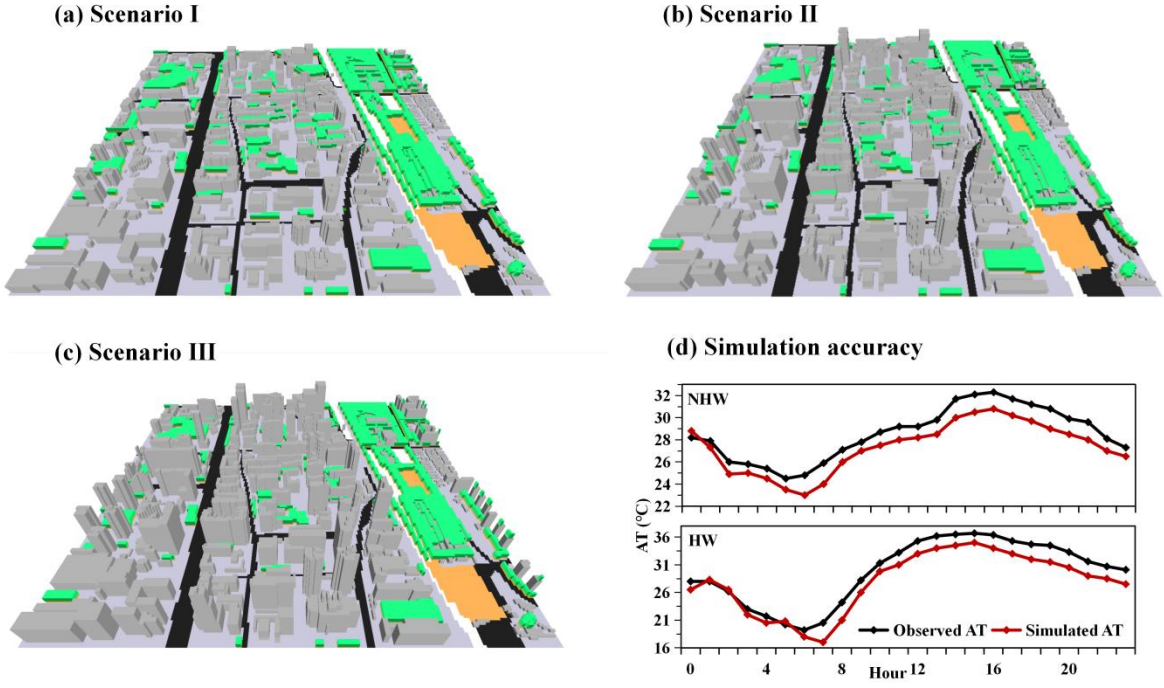

Figure: 9 Real scenario (a) and scenarios with reduced SVF (b-c) in the study area, and simulation errors (d).

This section selected a 500-meter radius area around Station 651061 on the North Fourth Ring Road as the simulation region, where the BCR was 0.225 and the SVF was 0.76. Three scenarios were set up: Scenario I was the real SVF (Figure 9a); based on the PDP analysis results of the machine learning model above, Scenario II was set with SVF=0.735 (the critical point of positive/negative effects, Figure 9b), and Scenario III was set with SVF=0.685 (the rapid growth stage of negative effects, Figure 9c). The ENVI-met model effectively simulated the diurnal variations of air temperature on days of NHW days (17 June 2020) and days of HW (15 June 15): the R^2 and RMSE for observed versus simulated air temperature (AT) were 0.64 and 1.25℃ on NHW days, and 0.73 and 1.16℃ on HW days, respectively. Compared with the findings of Morakinyo et al. (2018) and Tan et al. (2017), the correlation between simulated and observed values and the trend of temporal changes showed consistency. Due to the simplified treatment of building material heat capacity and environmental thermal radiation processes in the model (Ali-Toudert & Mayer, 2006), the simulated air temperatures were generally lower

https://doi.org/10.5194/egusphere-2025-2785
Preprint. Discussion started: 16 July 2025

than the measured values during the daytime. The difference between simulation and observation gradually narrowed after sunset, and the simulation error exceeded the measured value during 02:00–04:00. Overall, the trends of simulated and measured air temperature variation showed high consistency, indicating that the model could effectively reflect the diurnal characteristics of local urban thermal environments. Due to the simplified treatment of the heat capacity of building materials and environmental thermal radiation processes in the model (Ali-Toudert & Mayer, 2006), simulated air temperatures were generally lower than measured values during the daytime. The difference between simulated and observed air temperatures gradually narrowed after sunset, and simulation errors exceeded measured values between 02:00–04:00. Compared with the findings of Morakinyo et al. (2018) and Tan et al. (2017), the simulated AT in this study could effectively reflect the diurnal variations of the urban local thermal environment.

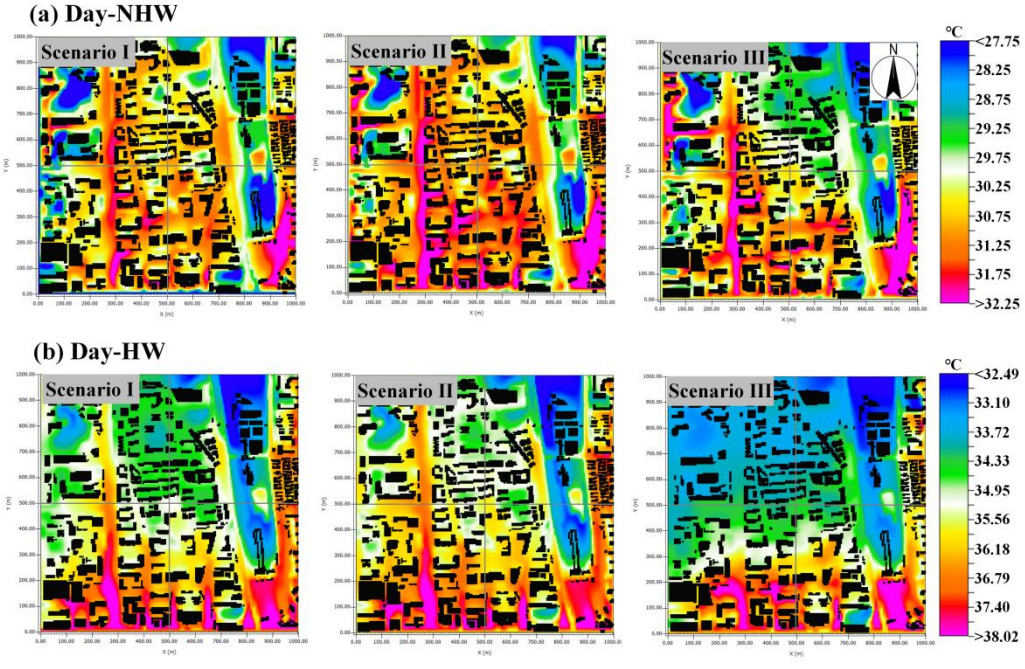

Figure: 10 Spatial distribution of the simulated AT in scenarios during daytime NHW (a) and HW (b) periods. The intersection of two gray crosshairs denotes the location of the meteorological station.

The figure above shows the simulated AT spatial distribution under different scenarios during daytime. During NHW periods (Figure 10a), the central point AT in Scenario II increased from 30.68℃ in Scenario I to 31.09℃, while that in Scenario III decreased to 30.33℃. During HW periods (Figure 10b), the central point air temperature in Scenario II increasedfrom 35.01℃ to 35.76℃. As SVF decreased, the obstruction of building clusters to air flow intensified, reducing the heat dissipation capacity. Meanwhile, blocking of long-wave radiation was exacerbated, promoting heat accumulation and leading to temperature increases. It should be noted that the central point AT in Scenario III dropped to 34.39℃,

https://doi.org/10.5194/egusphere-2025-2785
Preprint. Discussion started: 16 July 2025

300 possibly because an excessively low SVF significantly increased building shadow areas, enhancing the shading effect on solar radiation, thus reducing surface heat absorption and inhibiting temperature rise (Perini & Magliocco, 2014).

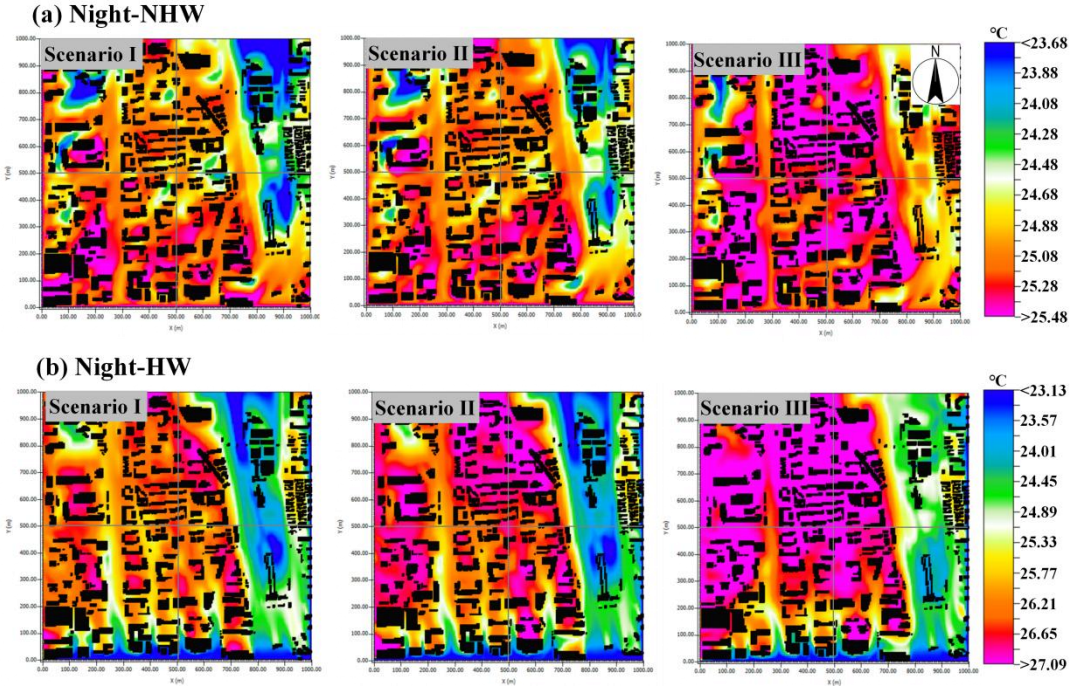

Figure: 11 Spatial distributions of the simulated AT across scenarios during NHW (a) and HW (b) periods at night .

305 Figure 11 shows the spatial distribution of the simulated AT indifferent scenarios at night. During NHW periods (Figure 11a), the central point AT in Scenario I was 24.86℃, increasing to 25.10℃ in Scenario II with a relatively small variation, while that in Scenario III increased significantly to 25.90℃. During HW periods (Figure 11b), the central point AT in Scenario I was 26.25℃, increasing to 26.83℃ in Scenario II and increased significantly to 27.93℃ in Scenario III. The increase in building height hinders the convective heat dissipation of nighttime air, making heat dissipation difficult and thus
310 promoting a significant temperature rise (Mo et al., 2024). Furthermore, the temperature differences between the scenarios during the HW periods were more significant than during the NHW periods, indicating that changes in building height have a more pronounced impact on air temperature during the HW periods, further amplifying the non-linear modulation of the building SVF in AT.

https://doi.org/10.5194/egusphere-2025-2785
Preprint. Discussion started: 16 July 2025

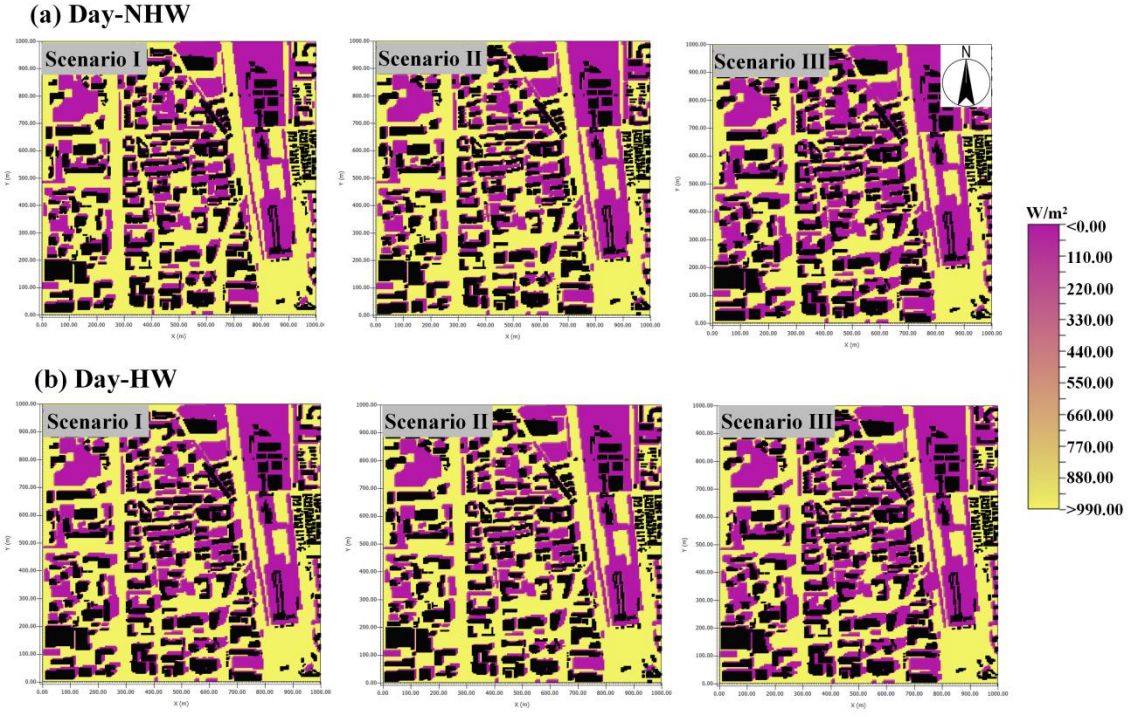

Figure: 12 Spatial distribution of simulated short-wave (SW) radiation across scenarios during daytime NHW (a) and HW (b) periods.

Combined with the spatial distribution of short-wave (SW) radiation, the temperature phenomena under different SVF daytime conditions can be further explained. Overall, SW radiation during HW periods is higher than during NHW periods (Figure 12). Specifically, in Scenario II during the HW periods (Figure 12b), the average SW radiation slightly decreases from 636.16 W/m² to 602.27 W/m², but AT shows an upward trend. This can be attributed to the obstruction of air flow by buildings (Ge et al., 2025), where the heat accumulation effect dominates in the competition between SW radiation attenuation caused by increased building height and air flow resistance. In Scenario III, the average SW radiation drops to 537.88 W/m², and significant shadow shading leads to a substantial reduction in SW radiation (Lin et al., 2024), thereby inhibiting the temperature rise. At night, the heat dissipation of LW radiation exhibits stronger non-linear threshold characteristics (Figure 13). In Scenario II during the HW periods (Figure 13b), the average LW radiation increases from 408.34 W/m² to 412.81 W/m². At this time, the resistance to escape of LW radiation is limited, so the air temperature only increases slightly. In Scenario III, the lower SVF significantly reduces the loss of LW radiation to the atmosphere, with the average LW radiation rapidly increasing to 424.31 W/m², accompanied by a noticeable temperatureincrease. This is because multiple reflections between building facades retain radiation energy within urban canyons, thus enhancing the capture of LW radiation (Mei et al., 2025). In summary, buildings exert nonlinear modulation on urban diurnal thermal environments

https://doi.org/10.5194/egusphere-2025-2785
Preprint. Discussion started: 16 July 2025

through the competitive effects of SW radiation shading and ventilation resistance, as well as the reflection and accumulation mechanisms of LW radiation.

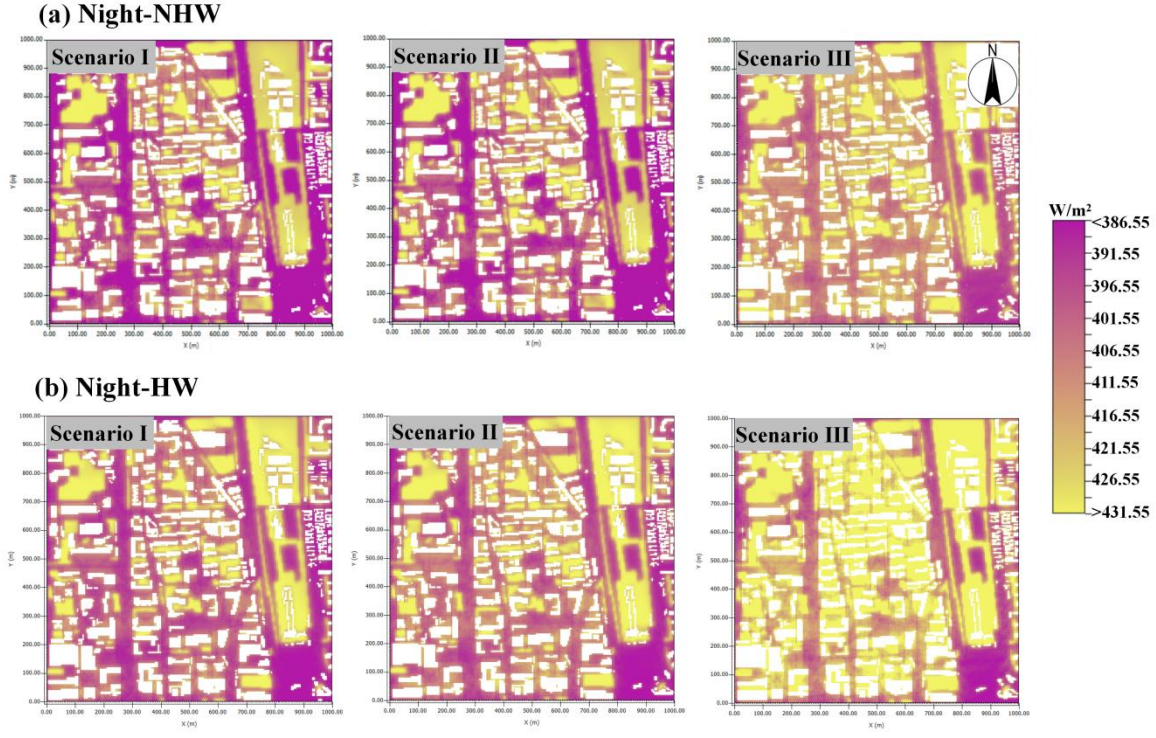

Figure: 13 Spatial distribution of simulated long-wave (LW) radiation across scenarios during nighttime NHW (a) and HW (b) periods.

4 Discussions

Urban morphology influences the CUHI by altering surface properties and spatial structures. As a dynamic meteorological factor, the inherent relationship between the wind field and CUHII should not be overlooked. This section analyzes the modulation mechanisms of the wind field on the diurnal CUHII during HW periods.

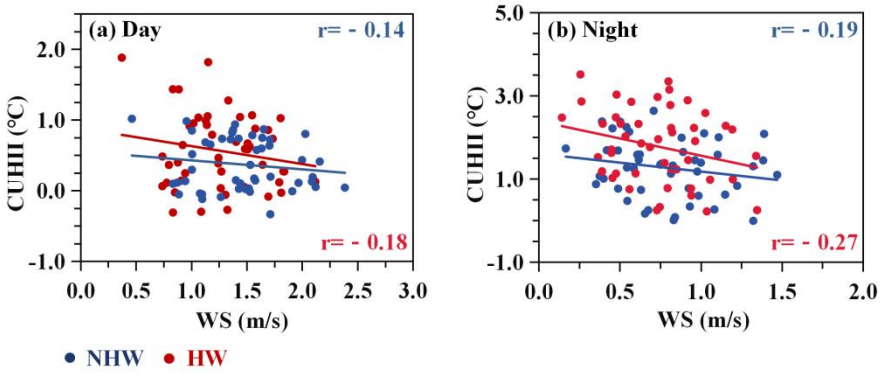

https://doi.org/10.5194/egusphere-2025-2785
Preprint. Discussion started: 16 July 2025

Figure 14: The correlation between wind speed (WS) and CUHII during NHW and HW periods: (a) daytime; (b) nighttime.

Figure 14a shows that during the daytime, the correlation coefficients (r) between WS and CUHII were -0.14 during NHW periods and -0.18 during HW periods, indicating a weak negative correlation that was slightly stronger during HW periods. Deng et al. (2025) simulated that a 10% increase in WS could reduce the CUHII by 0.16℃ during summer days. Stronger solar radiation during HW periods makes the heat dissipation effect of wind more significant for CUHII. During night (Figure 14b), the r was -0.19 during NHW periods and -0.27 during HW periods, with enhanced negative correlations compared to daytime, especially during HW periods. This may be related to the heat dissipation characteristics of the underlying urban surface during nighttime (Liu et al., 2022), where slower heat release makes the modulation of WS in CUHII more pronounced.

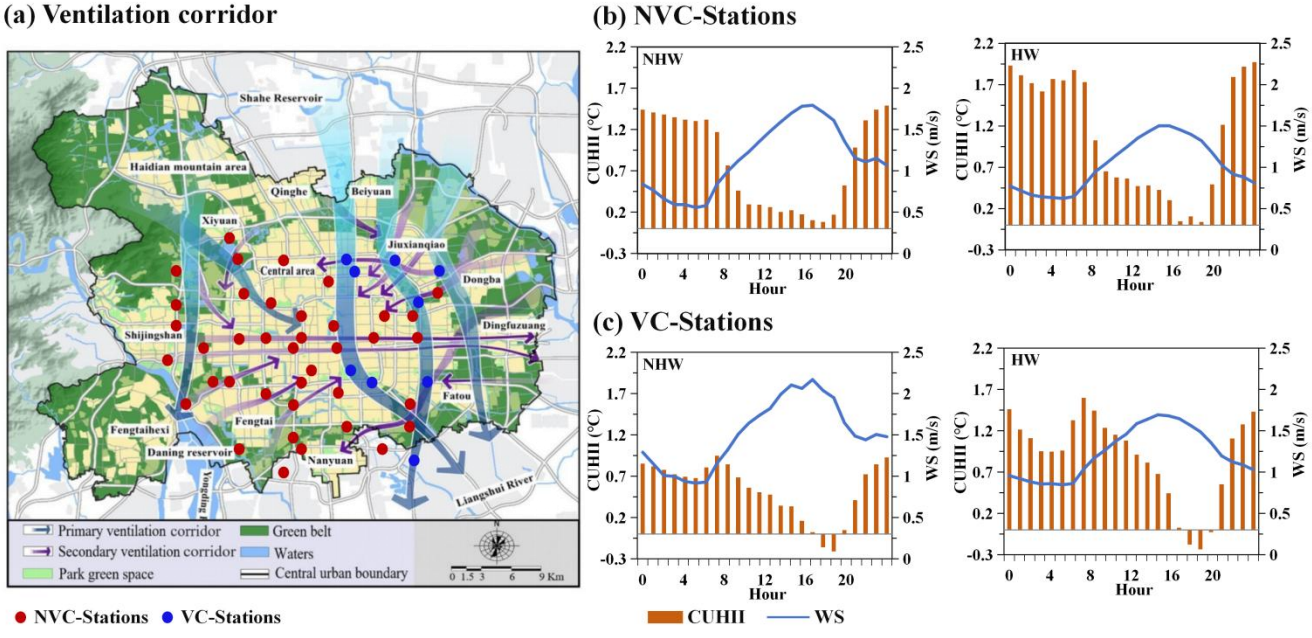

Figure 15: Impacts of ventilation corridors on diurnal variations of WS and CUHII. (a) Urban ventilation corridor planning in Beijing. Based on the Beijing Urban Master Plan, published by the Beijing Municipality Government. (b) Diurnal variations of WS and CUHII during NHW and HW periods at Non-Ventilation Corridor Stations (NVC-Stations). (c) Diurnal variations of WS and CUHII during NHW and HW periods at Ventilation Corridor Stations (VC-Stations).

Urban ventilation corridors represent an energy-efficient ecological approach to improving urban wind-thermal environments by taking advantage of natural meteorological conditions (Masmoudi & Mazouz, 2004; Masson, 2006; Palusci et al., 2021). In recent years, Beijing has proposed to construct ventilation corridors to alleviate increasingly severe urban environmental problems (Figure 15a). This section designates nine stations within first-level ventilation corridors as Ventilation Corridor Stations (VC-Stations) and the remaining 39 stations as Non-Ventilation Corridor Stations (NVC-

https://doi.org/10.5194/egusphere-2025-2785
Preprint. Discussion started: 16 July 2025

Stations). Data show that WS at NVC-Stations (Figure 15b) is significantly lower than that at VC-Stations (Figure 15c). For example, at night WS at NVC-Stations during HW periods remains around 0.5 m/s, whereas that at VC-Stations stays above 0.8 m/s. CUHII in VC-Stations generally exhibits an inverse relationship with WS. Taking NVC-Stations as an example, when WS is 0.5 m/s in the early morning during HW periods, CUHII reaches 1.9℃; when WS increases to 1.5 m/s in the afternoon, CUHII drops to only 0.3℃. In particular, the CUHII mitigation effect of ventilation corridors show significant diurnal differences. CUHII differences between the two station types are minimal during the daytime, possibly because high baseline WS reduces the heat mitigation effect of WS gains from ventilation corridors. During nighttime, however, with lower background WS, the WS enhancement from ventilation corridors is more pronounced (Hsieh & Huang, 2016), and the thermal environment is more sensitive to WS modulation (She et al., 2022), resulting in significantly lower nighttime CUHII at VC-Stations compared to NVC-Stations (42.09% lower during NHW periods and 33.91% lower during HW periods).

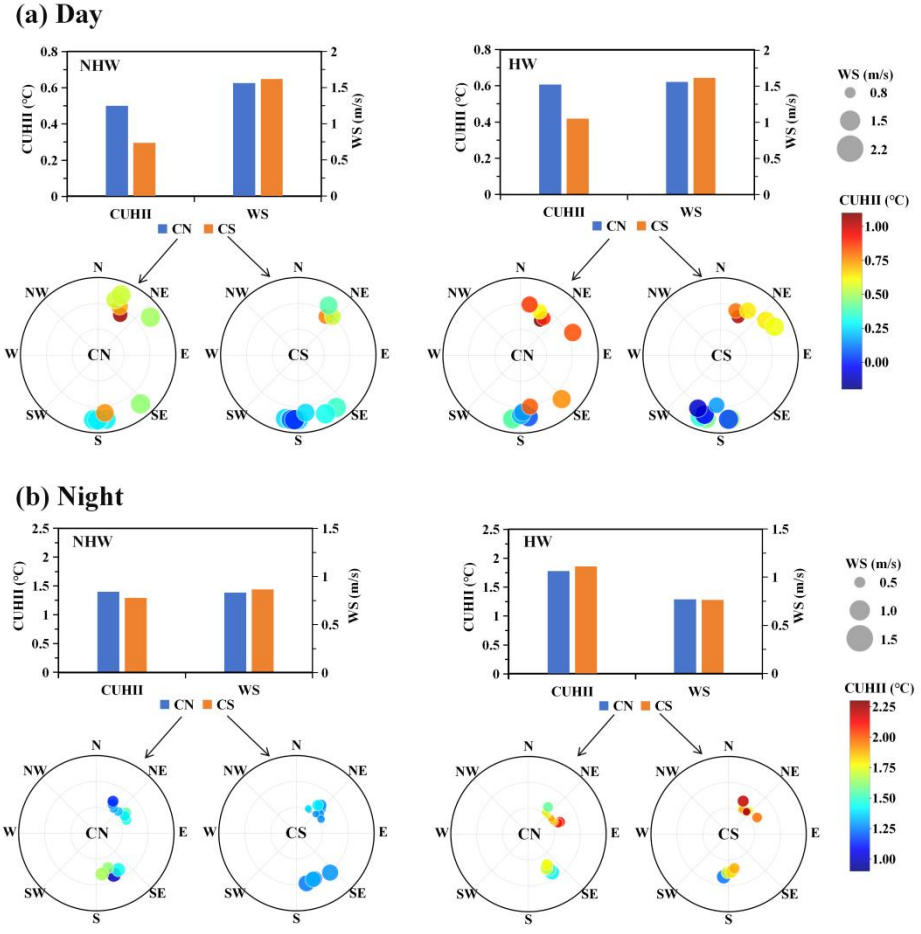

Figure 16: Diurnal CUHII and wind rose diagrams for city northern (CN) stations and city southern (CS) stations: (a) daytime; (b) nighttime. In the wind rose diagrams, bubble positions indicate wind direction, bubble sizes represent wind speed magnitudes, and bubble color intensity reflects CUHII strength.

https://doi.org/10.5194/egusphere-2025-2785
Preprint. Discussion started: 16 July 2025

The bar charts in Figure 16a show that during the daytime, the differences in WS between the CN (city northern) and CS (city southern) stations are minimal during both the NHW and HW periods. However, CUHII at CN stations is 0.49℃ during NHW and 0.61℃ during HW, significantly higher than 0.28℃ and 0.42℃ at CS stations, indicating that WS might not be the primary cause spatial patterns of CUHII. Wind transports heat through thermal advection in urban areas (Wang et al., 2020), potentially exacerbating the risks of thermal exposure in specific regions (Heaviside et al., 2015; Bassett et al., 2016). Beijing's typical mountain-valley wind circulation (Tian & Miao, 2019) shows predominant southerly winds (approximately 1.62 m/s) during the daytime, blowing from valleys to mountains. This stable high WS promotes horizontal heat transport from the upstream to downstream urban areas, increasing CUHII in northern urban regions. At night (Figure 16b), predominant northerly winds (approximately 0.75 m/s) blow from mountains to valleys, and the CUHII shows little difference between CN and CS stations. This phenomenon can be attributed to the WS threshold effect of horizontal heat transport. Weak prevailing winds stabilize the atmospheric stratification, thereby hindering urban heat dissipation, particularly during clear and light-wind nights (Kim & Baik, 2005). Studies further indicate that the CUHI center drifts downwind with increasing WS, with an average drift speed threshold—when WS is below this threshold, spatial differences in the urban thermal environment are primarily determined by local underlying surface properties (e.g., green space ratio, building density) (Xu et al., 2019). In summary, the impact of wind field on CUHII is jointly influenced by wind speed, direction, and source, with diurnal differences in modulation mechanisms: nighttime wind significantly mitigates CUHII, especially in ventilation corridor areas, while daytime prevailing winds may exacerbate thermal burdens in downstream regions through thermal advection rather than serving as simple cooling factors.

5 Conclusions

By integrating ground observations, machine learning, and microclimate simulation, this study systematically unveiled the diurnal response mechanisms of CUHII to urban morphology during HW periods in Beijing megacity. The findings demonstrated that CUHII during HW periods exhibited a significant enhancement compared to NHW periods, with a 91.3% increase during the daytime and a 52.7% increase during the nighttime. Its diurnal variation exhibited a U-shaped fluctuation, exhibiting substantial spatial variations (with the strongest fluctuation within the Second Ring Road during the day and the most prominent around the Fourth Ring Road at night). Machine learning analysis indicated that the BCR exhibited the highest significance for CUHII during the daytime, while the SVF played the most dominant role during the nighttime. The mean importance of 2D/3D morphological indicators increased by 16.2%–36.7% during HW periods, with interactive effects between BCR and SVF. ENVI-met simulations further confirmed the nonlinear modulation mechanism of urban morphology on thermal environments: when SVF decreased from 0.735 to 0.685, building modulation of daytime temperature was collaboratively influenced by SW radiation shading and ventilation resistance, showing a two-stage characteristic of first warming and then cooling; nighttime temperature changes were dominated by the reflection and accumulation of LW

https://doi.org/10.5194/egusphere-2025-2785
Preprint. Discussion started: 16 July 2025

radiation by buildings, exhibiting nonlinear characteristics of accelerated warming. Furthermore, the study identified notable diurnal variations in the impact of wind fields on CUHII: ventilation corridors could decrease CUHII by 33.91%–42.09% during nighttime hours, thus effectively mitigating CUHII; conversely, prevailing winds during daytime hours might intensify CUHII in downstream regions as a result of thermal advection, instead of merely acting as cooling elements. The findings furnish significant quantitative references for the optimization of urban morphology and the planning of ventilation corridors, providing precise scientific guidance for the mitigation of urban thermal risks.

Data availability. The hourly AWS observation data are available upon request from the China Meteorological Data Service Center (http://data.cma.cn/en). The land cover data are available at https://zenodo.org/record/5816591 (Yang & Huang, 2021).

Author contributions. TS and YY conceptualized the study. TS wrote the original manuscript and plotted all the figures. YY, PQ and SL assisted in the conceptualization and model development. All the authors contributed to the manuscript preparation, discussion, and writing.

Financial support. This research has been supported by the National Natural Science Foundation of China (grant nos. 42222503, 42030606, and 42105147), the Joint Research Project for Meteorological Capacity Improvement (grant no. 22NLTSQ013), and the Anhui Key Laboratory of Real Scene Geographical Environment Open Fund Project (grant no. 2024PEG010).

Competing interests. The contact author has declared that none of the authors has any competing interests.

References

Acero, J. A., Koh, E. J. Y., Ruefenacht, L. A., & Norford, L. K.: Modelling the influence of high-rise urban geometry on outdoor thermal comfort in Singapore, Urban Climate, 36, 100775, https://doi.org/10.1016/j.uclim.2021.100775, 2021.

Alavipanah, S., Schreyer, J., Haase, D., et al.: The effect of multi-dimensional indicators on urban thermal conditions, J. Clean. Prod., 177, 115–123, , 2018.

Ali-Toudert, F., Mayer, H.: Numerical study on the effects of aspect ratio and orientation of an urban street canyon on outdoor thermal comfort in hot and dry climate, Building and Environment, 41(2), 94–108, https://doi.org/10.1016/j.buildenv.2005.01.013, 2006.

https://doi.org/10.5194/egusphere-2025-2785
Preprint. Discussion started: 16 July 2025

Alonso, L., & Renard, F.: A new approach for understanding urban microclimate by integrating complementary predictors at different scales in regression and machine learning models, Remote Sensing, 12, 2434, https://doi.org/10.3390/rs12152434, 2020.

Ao, X., Wang, L., Zhi, X., Gu, W., Yang, H., Li, D.: Observed synergies between urban heat islands and heat waves and their controlling factors in Shanghai, China, Journal of Applied Meteorology and Climatology, https://doi.org/10.1175/JAMC-D-19-0073.1, 2019.

Bassett, R., Cai, X., Chapman, L., Heaviside, C., Thornes, J. E., Muller, C. L., & Warren, E. L.: Observations of urban heat island advection from a high-density monitoring network, Quarterly Journal of the Royal Meteorological Society, 142(699), 2434–2441, https://doi.org/10.1002/qj.2859, 2016.

Battista, G., et al.: Space-time estimation of the urban heat island in Rome (Italy): overall assessment and effects on the energy performance of buildings, Build. Environ., 228, 109878, https://doi.org/10.1016/j.buildenv.2022.109878, 2023.

Berardi, U., Jandaghian, Z., & Graham, J.: Effects of greenery enhancements for the resilience to heat waves: A comparison of analysis performed through mesoscale (WRF) and microscale (Envi-met) modeling, Science of the Total Environment, 747, 141300, https://doi.org/10.1016/j.scitotenv.2020.141300, 2020.

Berger, C., Rosentreter, J., Voltersen, M., Baumgart, C., Schmullius, C., & Hese, S.: Spatio-temporal analysis of the relationship between 2D/3D urban site characteristics and land surface temperature, Remote Sensing of Environment, 193, 225–243, https://doi.org/10.1016/j.rse.2017.02.020, 2017.

Chan, S. Y., & Chau, C. K.: On the study of the effects of microclimate and park and surrounding building configuration on thermal comfort in urban parks, Sustainable Cities and Society, 64, 102512, https://doi.org/10.1016/j.scs.2020.102512, 2021.

Chen, T., & Guestrin, C.: XGBoost: A scalable tree boosting system, in Proceedings of the 22nd ACM SIGKDD international conference on knowledge discovery and data mining, Association for Computing Machinery, https://doi.org/10.1145/2939672.2939785, 2016.

Cheval, S., Amihesei, V. A., Chitu, Z., et al.: A systematic review of urban heat island and heat waves research (1991–2022), Climate Risk Management, 44, 100603, https://doi.org/10.1016/j.crm.2024.100603, 2024.

Deng, Y. Z., Kong, X. F., Zhou, H. Z.: Field measurement and CFD simulation study on UHI in high-density blocks of Shanghai based on street canyons, Sustainable Cities and Society, 124, 106302, https://doi.org/10.1016/j.scs.2025.106302, 2025.

Di Giuseppe, E., Ulpiani, G., Cancellieri, C., Di Perna, C., D'Orazio, M., & Zinzi, M.: Numerical modelling and experimental validation of the microclimatic impacts of water mist cooling in urban areas, Energy and Buildings, 231, 110638, https://doi.org/10.1016/j.enbuild.2020.110638, 2021.

Ding, X., Zhao, Y., Strebel, D., et al.: A WRF-UCM-SOLWEIG framework for mapping thermal comfort and quantifying urban climate drivers: Advancing spatial and temporal resolutions at city scale, Sustainable Cities and Society, 112, 105628, https://doi.org/10.1016/j.scs.2024.105628, 2024.

https://doi.org/10.5194/egusphere-2025-2785
Preprint. Discussion started: 16 July 2025

Fallah Ghalhari, G., Dadashi Roudbari, A.: An investigation on thermal patterns in Iran based on spatial autocorrelation, Theor. Appl. Climatol., 131(3-4), 865–876, https://doi.org/10.1007/s00704-016-1957-8, 2018.

Forouzandeh, A.: Prediction of surface temperature of building surrounding envelopes using holistic microclimate ENVI-met model, Sustainable Cities and Society, 70, 102878, https://doi.org/10.1016/j.scs.2021.102878, 2021.

Gao, Y., Zhao, J., Yu, K.: Effects of block morphology on the surface thermal environment and the corresponding planning strategy using the geographically weighted regression model, Build. Environ., 216, 109037, https://doi.org/10.1016/j.buildenv.2022.109037, 2022.

Ge, J., Wang, Y., Guo, Y., et al.: Multiple-scale urban form renewal strategies for improving diffusion of building heat emission—A case in Xi'an, China, Energy & Buildings, 328, 115160, https://doi.org/10.1016/j.enbuild.2024.115160, 2025.

Ge, F., Zhang, L., Wang, J., Tian, G., & Feng, Y.: Multi-scale temporal characteristics and periodic analysis of urban heat island - a case study of Beijing, Journal of Beijing Normal University (Natural Science), 52(2), 210–215, , 2016.

Gosling, S. N., Lowe, J. A., McGregor, G. R., et al.: Associations between elevated atmospheric temperature and human mortality: a critical review of the literature, Climatic Change, 92(3-4), 299–341, https://doi.org/10.1007/s10584-008-9471-1, 2009.

Gu, X., Wu, Z., Liu, X., Qiao, R., & Jiang, Q.: Exploring the Nonlinear Interplay between Urban Morphology and Nighttime Thermal Environment, Sustainable Cities and Society, 101, 105176, https://doi.org/10.1016/j.scs.2024.105176, 2024.

Guo, F., Schlink, U., Wu, W., et al.: Scale-dependent and season-dependent impacts of 2D/3D building morphology on land surface temperature, Sustainable Cities and Society, 97, 104788, https://doi.org/10.1016/j.scs.2023.104788, 2023.

Guo, G., Zhou, X., Wu, Z., Xiao, R., & Chen, Y.: Characterizing the impact of urban morphology heterogeneity on land surface temperature in Guangzhou, China, Environmental Modelling & Software, 84, 427–439, https://doi.org/10.1016/j.envsoft.2016.06.021, 2016.

Han, D., An, H., Wang, F., Xu, X., Qiao, Z., Wang, M., et al.: Understanding seasonal contributions of urban morphology to thermal environment based on boosted regression tree approach, Building and Environment, 226, 109770, https://doi.org/10.1016/j.buildenv.2022.109770, 2022.

He, J., Shi, Y., Xu, L., Lu, Z., & Feng, M.: An investigation on the impact of blue and green spatial pattern alterations on the urban thermal environment: A case study of Shanghai, Ecological Indicators, 158, 111244, https://doi.org/10.1016/j.ecolind.2023.111244, 2024.

Heaviside, C., Cai, X. M., & Vardoulakis, S.: The effects of horizontal advection on the urban heat island in Birmingham and the West Midlands, United Kingdom during a heatwave, Quarterly Journal of the Royal Meteorological Society, 141(689), 1429–1441, https://doi.org/10.1002/qj.2549, 2015.

Henits, L., Mucsi, L., & Liska, C. M.: Monitoring the changes in impervious surface ratio and urban heat island intensity between 1987 and 2011 in Szeged, Hungary, Environ. Monit. Assess., 189(1), 1–13, https://doi.org/10.1007/s10661-017-6097-6, 2017.

https://doi.org/10.5194/egusphere-2025-2785
Preprint. Discussion started: 16 July 2025

Hong, T., Yim, S. H. L., & Heo, Y.: Interpreting complex relationships between urban and meteorological factors and street-level urban heat islands: Application of random forest and SHAP method, Sustainable Cities and Society, 126, 106353, https://doi.org/10.1016/j.scs.2025.106353, 2025.

Hsieh, C. M., & Huang, H. C.: Mitigating urban heat islands: A method to identify potential wind corridor for cooling and ventilation, Computers Environment and Urban Systems, 57, 130–143, https://doi.org/10.1016/j.compenvurbsys.2016.02.005, 2016.

Hu, D., Meng, Q. Y., Schlink, U., Hertel, D., Liu, W. X., Zhao, M. F., & Guo, F. X.: How do urban morphological blocks shape spatial patterns of land surface temperature over different seasons? A multifactorial driving analysis of Beijing, Sustainable Cities and Society, 84, 103648, https://doi.org/10.1016/j.scs.2022.103648, 2022.

Huang, X., & Wang, Y.: Investigating the effects of 3D urban morphology on the surface urban heat island effect in urban functional zones by using high-resolution remote sensing data: a case study of Wuhan, Central China, ISPRS J. Photogrammetry Remote Sens., 152, 119–131, https://doi.org/10.1016/j.isprsjprs.2019.05.014, 2019.

IPCC: Climate Change 2021: The physical science basis. Contribution of working group I to the sixth assessment report of the intergovernmental panel on climate change, Cambridge University Press, Cambridge and New York, , 2021.

Jiang, S., Lee, X., Wang, J., & Wang, K.: Amplified urban heat islands during heat wave periods, Journal of Geophysical Research: Atmospheres, 124, 7797–7812, https://doi.org/10.1029/2018JD030230, 2019.

Jiang, Y., Zhou, H., Zhou, X., & Chen, X.: Evaluating the impact of urban morphology on urban vitality: an exploratory study using big geo-data, INTERNATIONAL JOURNAL OF DIGITAL EARTH, 17(1), 2327571, https://doi.org/10.1080/17538947.2024.2327571, 2024.

Kim, Y. H., & Baik, J. J.: Spatial and temporal structure of the urban heat island in Seoul, J Appl Meteor, 44(5), 591–605, , 2005.

Kong, F., Sun, C. F., Liu, F. F., Yin, H. W., Jiang, F., Pu, Y. X., et al.: Energy saving potential of fragmented green spaces due to their temperature regulating ecosystem services in the summer, Applied Energy, 183, 1428–1440, https://doi.org/10.1016/j.apenergy.2016.09.070, 2016.

Li, Z., & Hu, D.: Exploring the relationship between the 2D/3D architectural morphology and urban land surface temperature based on a boosted regression tree: A case study of Beijing, China, Sustainable Cities and Society, 78, 103392, https://doi.org/10.1016/j.scs.2022.103392, 2022.

Lin, Z., Xu, H., Han, L., et al.: Day and night: Impact of 2D/3D urban features on land surface temperature and their spatiotemporal non-stationary relationships in urban building spaces, Sustainable Cities and Society, 108, 105507, https://doi.org/10.1016/j.scs.2024.105507, 2024.

Liu, M., Ma, J., Zhou, R., et al.: High-resolution mapping of mainland China's urban floor area, Landsc. Urban Plann., 214, 104187, https://doi.org/10.1016/j.landurbplan.2021.104187, 2021.

https://doi.org/10.5194/egusphere-2025-2785
Preprint. Discussion started: 16 July 2025

Liu, X., Wu, T., Jiang, Q., et al.: The nonlinear climatological impacts of urban morphology on extreme heats in urban functional zones: An interpretable ensemble learning-based approach, Building and Environment, 273, 112728, https://doi.org/10.1016/j.buildenv.2025.112728, 2025.

Liu, Y. C., Huang, Y. D., Zhang, Z., Wang, K. X., Luo, Y., & Cui, P. Y.: Impacts of green walls on the characteristics of thermo-flow and photochemical reaction kinetics within street canyons, Urban Forestry & Urban Greening, 72, 127568, https://doi.org/10.1016/j.ufug.2022.127568, 2022.

Lundberg, S., & Lee, S. I.: A Unified Approach to Interpreting Model Predictions, , https://doi.org/10.48550/arXiv.1705.07874, 2017.

Luo, Y., Wu, Z., Wong, M. S., Yang, J., & Jiao, Z.: Simulating the impact of ventilation corridors for cooling air temperature in local climate zone scheme, Sustainable Cities and Society, 115, 105848, https://doi.org/10.1016/j.scs.2024.105848, 2024.

Masmoudi, S., & Mazouz, S.: Relation of geometry, vegetation and thermal comfort around buildings in urban settings, the case of hot arid regions, Energy and Buildings, 36(7), 710–719, https://doi.org/10.1016/j.enbuild.2004.01.043, 2004.

Masson, V.: Urban surface modeling and the meso-scale impact of cities, Theoretical and Applied Climatology, 84, 35–45, https://doi.org/10.1007/s00703-005-0182-1, 2006.

Mei, S.-J., Chen, G., Wang, K., & Hang, J.: Parameterizing urban canopy radiation transfer using three-dimensional urban morphological parameters, Urban Climate, 60, 102363, https://doi.org/10.1016/j.uclim.2025.102363, 2025.

Meng, Q., Gao, J., Zhang, L., et al.: Coupled cooling effects between urban parks and surrounding building morphologies based on the microclimate evaluation framework integrating remote sensing data, Sustainable Cities and Society, 102, 105235, https://doi.org/10.1016/j.scs.2024.105235, 2024.

Mo, Y., Bao, Y., Wang, Z., et al.: Spatial coupling relationship between architectural landscape characteristics and urban heat island in different urban functional zones, Building and Environment, 257, 111545, https://doi.org/10.1016/j.buildenv.2024.111545, 2024.

Morakinyo, T. E., Dahanayake, K., Adegun, O. B., & Balogun, A. A.: Modelling the effect of tree-shading on summer indoor and outdoor thermal condition of two similar buildings in a Nigerian university, Energy and Buildings, 130, 721–732, https://doi.org/10.1016/j.enbuild.2016.08.087, 2016.

Ng, E., Yuan, C., Chen, L., Ren, C., & Fung, J. C. H.: Improving the wind environment in high-density cities by understanding urban morphology and surface roughness: a study in Hong Kong, Landsc. Urban Plan., 101(1), 59–74, https://doi.org/10.1016/j.landurbplan.2011.03.007, 2011.

Ngarambe, J., Nganyiyimana, J., Kim, I., Santamouris, M., & Yunid, G. Y.: Synergies between urban heat island and heat waves in Seoul: The role of wind speed and land use characteristics, PLoS ONE, 15(12), e0243571, https://doi.org/10.1371/journal.pone.0243571, 2020.

Nugroho, N. Y., Triyadi, S., & Wonorahardjo, S.: Effect of high-rise buildings on the surrounding thermal environment, Building and Environment, 207, 108393, https://doi.org/10.1016/j.buildenv.2021.108393, 2022.

https://doi.org/10.5194/egusphere-2025-2785
Preprint. Discussion started: 16 July 2025

Oke, T. R.: Initial guidance to obtain representative meteorological observations at urban sites, University of British Columbia, Vancouver, , 2004.

Palusci, O., Monti, P., Cecere, C., Montazeri, H., & Blocken, B.: Impact of morphological parameters on urban ventilation in compact cities: the case of the Tuscolano-Don Bosco district in Rome, Science of The Total Environment, 807, 150490, https://doi.org/10.1016/j.scitotenv.2021.150490, 2022.

Perini, K., & Magliocco, A.: Effects of vegetation, urban density, building height, and atmospheric conditions on local temperatures and thermal comfort, Urban Forestry & Urban Greening, 13(3), 495–506, https://doi.org/10.1016/j.ufug.2014.03.003, 2014.

Ramamurthy, P., & Bou-Zeid, E.: Heatwaves and urban heat islands: a comparative analysis of multiple cities, Journal of Geophysical Research: Atmospheres, 122(1), 168–178, https://doi.org/10.1002/2016JD025588, 2017.

Ryu, Y. H., & Baik, J. J.: Quantitative analysis of factors contributing to urban heat island intensity, Journal of Applied Meteorology & Climatology, 51(5), 842–854, https://doi.org/10.1175/JAMC-D-11-098.1, 2012.

Scarano, M., & Mancini, F.: Assessing the relationship between sky view factor and land surface temperature to the spatial resolution, International Journal of Remote Sensing, 38(20), 6910–6929, https://doi.org/10.1080/01431161.2017.1368099, 2017.

Shao, L., Liao, W., Li, P., Luo, M., Xiong, X., & Liu, X.: Drivers of global surface urban heat islands: surface property, climate background, and 2D/3D urban morphologies, Build. Environ., 242, 110581, https://doi.org/10.1016/j.buildenv.2023.110581, 2023.

She, Y., Liu, Z., Zhan, W., et al.: Strong regulation of daily variations in nighttime surface urban heat islands by meteorological variables across global cities, Environmental Research Letters, 17(1), 014049, https://doi.org/10.1088/1748-9326/ac4630, 2022.

Shi, T., Sun, D. B., Huang, Y., Lu, G. P., & Yang, Y. J.: A new method for correcting urbanization-induced bias in surface air temperature observations: Insights from comparative site-relocation data, Frontiers in Environmental Science, 9, 62541, https://doi.org/10.3389/fenvs.2021.62541, 2021.

Shi, T., Yang, Y., Qi, P., Ren, G., Wen, X., & Gul, C.: Adjustment of the urbanization bias in surface air temperature series based on urban spatial morphologies and using machine learning, Urban Climate, 55, 101991, https://doi.org/10.1016/j.uclim.2024.101991, 2024.

Tan, Z., Lau, K. K. L., & Ng, E.: Planning strategies for roadside tree planting and outdoor comfort enhancement in subtropical high-density urban areas, Building and Environment, 120, 93–109, https://doi.org/10.1016/j.buildenv.2017.05.017, 2017.

Tian, Y., & Miao, J.: Overview of mountain-valley breeze studies in China, Meteorological Science and Technology, 47(1), 1–11, https://doi.org/10.19517/j.1671-6345.20170777, 2019.

Tian, Y., Zhou, W., Qian, Y., Zheng, Z., & Yan, J.: The effect of urban 2D and 3D morphology on air temperature in residential neighborhoods, Landscape Ecology, 34(5), 1161–1178, https://doi.org/10.1007/s10980-019-00834-7, 2019.

https://doi.org/10.5194/egusphere-2025-2785
Preprint. Discussion started: 16 July 2025

Wang, L., Hou, H., & Weng, J.: Ordinary least squares modelling of urban heat island intensity based on landscape composition and configuration: a comparative study among three megacities along the Yangtze River, Sustain. Cities Soc., 62, 102381, https://doi.org/10.1016/j.scs.2020.102381, 2020.

Wang, Q., Wang, H., Ren, L., et al.: Hourly impact of urban features on the spatial distribution of land surface temperature: A study across 30 cities, Sustainable Cities and Society, 113, 105701, https://doi.org/10.1016/j.scs.2024.105701, 2024.

Wang, W., Yao, X., & Shu, J.: Air advection induced differences between canopy and surface heat islands, Science of the Total Environment, 725, 138120, https://doi.org/10.1016/j.scitotenv.2020.138120, 2020.

Wu, W.-B., Yu, Z.-W., Ma, J., & Zhao, B.: Quantifying the influence of 2D and 3D urban morphology on the thermal environment across climatic zones, Landscape and Urban Planning, 226, 104499, https://doi.org/10.1016/j.landurbplan.2022.104499, 2022.

Xu, D., Zhou, D., Wang, Y., Xu, W., & Yang, Y.: Field measurement study on the impacts of urban spatial indicators on urban climate in a Chinese basin and static-wind city, Build. Environ., 147, 482–494, https://doi.org/10.1016/j.buildenv.2018.11.015, 2019.

Xu, W. H., Li, Q. X., Wang, X. L., Yang, S., Cao, L., & Feng, Y.: Homogenization of Chinese daily surface air temperatures and analysis of trends in the extreme temperature indices, Journal of Geophysical Research: Atmospheres, 118(17), 9708–9720, https://doi.org/10.1002/jgrd.50791, 2013.

Xu, W., Zhang, L., Qi, L. B., et al.: Observation analysis of the influence of surface wind on urban heat island in Shanghai, Meteor Mon, 45(9), 1262–1277, , 2019.

Xue, J., Zong, L., Yang, Y., Bi, X., Zhang, Y., & Zhao, M.: Diurnal and interannual variations of canopy urban heat island (CUHI) effects over a mountain-valley city with a semi-arid climate, Urban Climate, 48, 101425, https://doi.org/10.1016/j.uclim.2023.101425, 2023.

Yang, P., Liu, W., Zhong, J., & Yang, J.: Evaluating the quality of temperature measured at automatic weather stations in Beijing, Journal of Applied Meteorological Science, 22(6), 706–715, https://doi.org/1001-7313(2011)22:6<706:BJDQZD>2.0.TX;2-2, 2011.

Yang, Y., Guo, M., Wang, L., Zong, L., Liu, D., Zhang, W., et al.: Unevenly spatiotemporal distribution of urban excess warming in coastal Shanghai megacity, China: Roles of geophysical environment, ventilation and sea breeze, Building and Environment, 235, 110180, https://doi.org/10.1016/j.buildenv.2023.110180, 2023.

Yang, Y., Zheng, X., Gao, Z., Wang, H., Wang, T., Li, Y., et al.: Long-term trends of persistent synoptic circulation events in planetary boundary layer and their relationships with haze pollution in winter half year over Eastern China, Journal of Geophysical Research: Atmospheres, 123, 10991–11007, https://doi.org/10.1029/2018JD028982, 2018.

Yin, C., Yuan, M., Lu, Y., Huang, Y., & Liu, Y.: Effects of urban form on the urban heat island effect based on spatial regression model, The Science of the total environment, 634, 696–704, https://doi.org/10.1016/j.scitotenv.2018.03.337, 2018.

https://doi.org/10.5194/egusphere-2025-2785
Preprint. Discussion started: 16 July 2025

Yin, H., & Zhao, X.: Urban heat island analysis based on high resolution measurement data: A case study in Beijing, Sustainable Cities and Society, 106, 105389, https://doi.org/10.1016/j.scs.2024.105389, 2024.

Zhang, M., Kafy, A.-A., Xiao, P., Han, S., Zou, S., Saha, M., Zhang, C., & Tan, S.: Impact of urban expansion on land surface temperature and carbon emissions using machine learning algorithms in Wuhan, China, Urban Climate, 47, 101347, https://doi.org/10.1016/j.uclim.2022.101347, 2023.

Zheng, Z., Ren, G., Wang, H., Dou, J., Gao, Z., Duan, C., et al.: Relationship between fine-particle pollution and the urban heat island in Beijing, China: Observational evidence, Boundary-layer Meteorology, 169, 93–113, https://doi.org/10.1007/s10546-018-0362-6, 2018.